Received: 1 May 2023 | Revised: 31 August 2023 | Accepted: 13 October 2023

DOI: 10.1002/prep.202300110

Propellants, Explosives, Pyrotechnics

RESEARCH ARTICLE

Calibration and uncertainty quantification for Davis Equation of State models for the High Explosive PBX 9501 products

Stephen A. Andrews[1] | **Jeffery A. Leiding**[2] | **Jasper Thrussell**[1] | **Christopher Ticknor**[2]

[1]XPC-8: Verification and Analysis, Los Alamos National Laboratory, Los Alamos NM, U.S.A.

[2]T-1: Physics and Chemistry of Materials, Los Alamos National Laboratory, Los Alamos NM, U.S.A.

Correspondence
Stephen A. Andrews, XPC-8: Verification and Analysis, Los Alamos National Laboratory, P. O. Box 1663, 87545, Los Alamos NM, U.S.A..
Email: saandrews@lanl.gov

Funding information
U.S. Department of Energy

Abstract

This paper investigates the uncertainty in the parameters used in the calibration of an Davis Equation Of State (EOS) for the detonation products of the High Explosive PBX 9501. The procedure sought to make use of all available information about this HE to inform the best set of calibration parameters as well as the uncertainty in these parameters. The procedure made use of historical experimental data, the results from thermo-chemical modeling as well as data on the best isentrope function fit to cylinder test experimental data. Combining all these heterogeneous data sources together in a Bayesian calibration, yielded a posterior mean and covariance. Sampling from the posterior distribution and evaluating an important Quantity Of Interest (QOI) in the EOS model, the detonation speed of a one-inch rate stick, produced a distribution which showed variations which were in agreement with experiments. The uncertainty in the EOS was reported as eleven sets of model calibrations which spanned the range of this QOI.

KEYWORDS
Bayesian, Calibration, High Explosives, PBX 9501, Uncertainty Quantification

1 | INTRODUCTION

Computer simulations of complex engineered systems require physics models to emulate the behavior of real physical processes which occur at length and time scales too small to be resolved on the computational grid. Such models are often parametric models with a fixed functional form and a small set of adjustable parameters, some of which are directly measurable physical properties and some of which are arbitrary fitting parameters. Though semi-parametric models such as B-splines [1], and neural networks exist, they cannot be easily included in a simulation without intrusive changes to the code. For these reasons, a set of parameters for existing functional forms is needed which gives the best agreement with experimental observations over a wide range of conditions. However, since the model is an approximation of a real process, there is uncertainty in these parameters and ideally sets of parameters which span the uncertainty in the model should be provided. With such sets of parameters a complex simulation of interest can be run multiple times in order to understand how uncertainty in the model's parameters affects a quantity of interest in the simulation.

This work focuses on models for the Equation Of State (EOS) for the detonation products of the High Explosive (HE) PBX 9501[1] using a functional form proposed by Davis [2–4]. This *Davis Products* functional form has changed slightly over time and in this work we will be using the functions as defined in [5]. One of the most important properties of an explosive is the speed at which an unsupported detonation wave can propagate through a charge of infinite diameter. This is the Chapman Jouguet (CJ) detonation speed, and has been the focus of historical measurements of HE performance. For any calibration to be useful, it must match experimental observations of D_{cj}.

Historical observations of HE performance have also included measurements of the Hugoniot[2] [6,7] and sound speed [6] at various overdriven states.

However, specifying D_{cj} alone is not sufficient to model HE performance, the behavior of the gases produced from reacting HE, the 'detonation products' or 'products' must be characterized at states both much higher in pressure than the CJ state and down to near-atmospheric pressures. Thermo-chemical codes use a ′physics-based′ approach to model the behavior of products gases and can predict their behavior to a reasonable degree of accuracy. These results, however, are not perfect and have been shown to not predict the CJ state exactly and can fail to precisely predict the detonation energy, affecting how much work the HE can transfer to a metal. Additionally, thermo-chemical codes are too expensive to run within hydrodynamic simulation software (*hydro-code*) and the EOS response must be approximated with either a tabular model or parametric function.

Hydro-codes can be used to predict the behavior of dynamic experiments where HE is accelerating a metal. A common experiment for inferring HE EOS is the *cylinder test* where a charge, typically 1 inch in diameter, is placed in a metal, typically copper, cladding and detonated [8,9]. The resulting motion of the wall is observed and this can be used to infer the behavior of the HE. Previous work [10] has presented methods of fitting a high dimensional B-spline function to cylinder test data to solve the inverse problem of finding the functional pressure-velocity relationship implied by the observed velocity-time history.[3] Though this approach gives excellent agreement with the experimental observations from a cylinder test, the results are not in a parametric or tabular form which can easily be shared or incorporated into a hydro-code.

This work aims to combine all three approaches: historical data, thermo-chemical modeling, and hydrodynamic simulation to obtain a set of parameters that is the best fit to all available data about the HE as well as a distribution of these parameters which characterizes our understanding of the uncertainty in them. The sequence of analysis that are as follows:

1. Identify the mean CJ detonation speed from historical records.
2. Use the thermo-chemical code magpie [11] to generate thermodynamic loci and a CJ state which matches historical data.
3. Use this CJ state to inform a prior for the cylinder test inversion problems.
4. Invert each cylinder test independently and produce a table of data from the CJ isentrope with correlated uncertainty.
5. Fit the parameters of a Davis Products equation of state to a set of data from historic observations, magpie data, and the isentrope data given by the cylinder test inversion.
6. Estimate the uncertainty in this EOS arising from the experiments and compare it to known variations in historical data.

These major steps are addressed in the following sections. Section 2 discusses the historic sources of HE data. Section 3 describes the thermo-chemical modeling tools, how they were used, and what data were extracted. Section 4 describes the setup of the cylinder inversion problem and the results of this study are presented in Section 6.1. The calibration problem for the Davis Products EOS model is described in Section 5 and the results are shown in Section 6.2. The uncertainty quantification process and results are shown in 6.3.

2 | HISTORIC HE DATA

The results of several decades of D_{cj} measurements are compiled in [12]. The detonation speed is sensitive to initial density, so to compare the measurements to eachother they must be corrected to the nominal density of PBX 9501, 1.836 $\mathrm{g\,cm^{-3}}$, using (1). [13]

$$\mathrm{D} = 1.60\,\mathrm{km\,s^{-1}} + (3.62\,\mathrm{km\,cm^3\,s^{-1}\,g^{-1}})\rho \tag{1}$$

After applying this transformation the mean of the data was 8.7959 $\mathrm{km\,s^{-1}}$ and the standard deviation was 6.3814 $\mathrm{m\,s^{-1}}$.

[1] A Plastic Bonded eXplosive (PBX) made up of 95% HMX (1,3,5,7-Tetranitro-1,3,5,7-tetrazocane) and 5% binder

[2] A locus of points which conserve mass momentum and energy across a shock from a given reference state

[3] This process is referred to as *inverting the cylinder test.*

These detonation speeds were measured in one-inch (25.4 mm) diameter rate sticks. The fact that these measurements were for finite-diameter rate sticks means they will differ slightly from the true *thermodynamic* detonation speed. Fritz *et al.* propose a detonation speed of $8.802\,\mathrm{km\,s^{-1}}$ [6] and Aslam and Short propose $8.811\,\mathrm{km\,s^{-1}}$. Applying the correction factor from [14] gives a conversion factor of $\frac{D_{cj}}{D_1} = 0.998445$; this changes the mean of the experimental detonation speeds to $8.810\,\mathrm{km\,s^{-1}}$, falling within the two estimates. This is the value which will be used as the thermodynamic detonation speed which the detonation products models will seek to match.

In addition to measurements of the CJ detonation speed, other historic data include measurements of the Hugoniot state and sound speeds. Fritz *et al.* measured both the shock speed on the Hugoniot as well as the sound speed at over-driven states [6]. Pittman *et al.* also measured the shock speed on the Hugoniot [7].

3 | THERMO-CHEMICAL MODELING

The magpie thermo-chemical code uses models for the Gibb's free energy to find an equilibrium mixture of the component gases of the detonation products. The free energy was modeled as the sum of contributions from ideal and non-ideal behavior, in a manner similar to other thermo-chemical codes [15]. The parameters for the ideal models could be obtained exactly from the open literature [11]. The non-ideal behavior of the interactions was modeled using Ross perturbation theory [16] sources for the calibrations for the interaction potentials used in this theory are listed in Table 1 of [11]. In short, many of the molecular potentials used in magpie were not tuned to match HE data, but were fit to experimental data of individual molecules; however, several of the interaction potentials employed derive from unpublished work, and lack full documentation.

The detonation products for PBX 9501 were modeled as a mixture of the following gases: N_2, H_2O, CO_2, CO, NH_3, NO, N_2O, NO_2, H_2, O_2, HCOOH, HCNO, CH_4, C_2H_2, C_2H_6, C_2N_2, O, H, N and C. There were three phases of carbon modeled: diamond, graphite and liquid diamond as described in [17]. Though there was some free carbon in the detonation products which was modeled, the abundance of free carbon was much less than in other explosives, such as triaminotrinitrobenzene (TATB) based HE formulations. For these reasons, the kinetics of carbon clustering were not considered in detail in the thermochemical model.The thermodynamic data generated by magpie and used in the calibration were all high temperature data and we anticipate chemical kinetics to be active and not "frozen".

A SESAME [18] EOS table was generated using magpie without any adjustment of the parameters and an example cylinder test was run. A comparison of the simulation and experiment is shown in Figure 4. The magpie simulation under-predicts the final speed of the wall, showing the model was creating an under-energetic EOS. However, the agreement is impressive considering that this EOS model is based on physics based calculations.

Using the default parameters, the detonation speed predicted by magpie was $8.829\,\mathrm{km\,s^{-1}}$, higher than the mean of the experimental data. The heat of formation for the PBX 9501 was adjusted down by $\approx 20\,\%$ until the detonation speed matched the target value. Magpie was then used to generate data which could supplement experiments in calibrating an equation of state model. Without adjusting the heat of formation, there was no single calibration which would agree with experimental data, cylinder test inversions and magpie data.

Using the tuned model, the pressure, temperature, and density at the CJ state was evaluated. Additionally, an isotherm along the CJ temperature was created for use in the subsequent calibration, described in Section 5.

TABLE 1 Tuned hyper-parameters for scaling the experimental uncertainties

Experiment	Uncertainty scaling factor
Hugoniots	1.0
Sound Speed	2.5
Cylinders K12-17229–K12-17233	4.0
Cylinder 8–1964	2.5
Cylinder 8–1932	4.0

4 | CYLINDER TEST INVERSION

A Bayesian approach was used to solve the inverse problem of identifying an isentrope function given observations of the wall velocity of an expanding cylinder filled with HE. The details of this Bayesian approach have been discussed previously in [10]. The cylinder tests were simulated using the Lagrangian hydrodynamic code FLAG [19]. The copper was modeled using an analytic equation of state model from [20] and a Preston-Tonks-Wallas material strength model using the calibration from [21].

The experimental observations took the form of time-dependent measurements of the cylinder wall velocity. The isentrope was represented by a set of B-splines. The optimization was constrained by the known physical

behavior of an EOS with no phase change: the function must be positive as well as monotonic and convex in specific volume.[4] [22] To construct a complete equation of state a model for the Grüneisen gamma was needed as well as a model for the isentrope. In the present analysis, the Grüneisen gamma model was also subject to inference. A model where the Grüneisen gamma was constant (*i.e.* independent of density) was chosen due to its simplicity and the fact that the thermodynamic trajectory of the HE detonation products on the cylinder should closely follow an isentrope as the short timescales of the problem do not allow significant heat transfer and thus the problem is nearly isentropic after the initial shock. Since the Grüneisen gamma only models behavior off the reference curve, (in this case an isentrope,) the results should not be overly sensitive to the choice of model; this assumption will be re-examined after the cylinder test inversions are performed.

Additionally, the Bayesian analysis considers not only the agreement between the EOS and the cylinder test but also the agreement between D_{cj} on the isentrope and historical data. This was necessary as the presence of the copper cladding meant that the velocity history is not strongly informative of the CJ state, so the CJ state of the optimal isentrope could disagree by more than the standard deviation with the historical mean if this was not considered in the Bayesian analysis.

4.1 | Priors

4.1.1 | Isentrope

The isentrope was modeled in a B-spline basis. The 75 knots were equi-log spaced between $0.01\,\mathrm{g\,cm^{-3}}$ and $4\,\mathrm{g\,cm^{-3}}$. The correlation in the prior was specified the distance in log-space between 2.4 knots with a fractional uncertainty of 0.25. These were the parameters used in a previous calibration of PBX 9501 [10]. There were 15 eigenfunctions with nonzero eigenvalues associated with this B-spline basis and correlation. The coefficients of these eigenfunctions were the degrees of freedom, θ of this semi-parametric model.

The prior for the isentrope was chosen to be a two term polynomial with fixed exponent values, designed to match the expected behavior at low and high densities. For pressures below the lower bound of the B-spline basis the pressure-density relationship was modeled as a power law, $P(\rho) = C\left(\frac{\rho}{0.01\ g\ cm^{-3}}\right)^{\gamma}$, fit to preserve $C1$ continuity at the lower bound of the B-spline basis. At these low densities it is expected that the polytropic expansion coefficient, γ, should be close to $\frac{6}{5}$ so this was chosen as the prior for these low density regions. Likewise, a rough approximation for HE behavior at densities near the CJ state is to use $\gamma = 3$. The chosen functional form for the prior, (2), blends between these two power laws.

$$P(\rho) = A\left(\frac{\rho}{\rho_o}\right)^{3} + B\left(\frac{\rho}{\rho_o}\right)^{\frac{6}{5}} \tag{2}$$

At the CJ state the isentrope is tangent to the Rayleigh line, $R(\rho) = \rho_o^2 D_{cj}^2\left(\rho_o^{-1} - \rho^{-1}\right) + P_o$. Given these two equations, and their derivatives, the coefficients A and B could be solved for as a function of the reference density ρ_o, D_{cj}, and the density of the CJ point ρ_{cj}, which was obtained from thermo-chemical analysis.

$$A = \frac{6D_{cj}^2\rho_o^4\rho_{cj} + 6D_{cj}\rho_o^3\rho_{cj} - 11D_{cj}^2\rho_o^5}{9\rho_{cj}^4} \tag{3}$$

$$B = \frac{5\left(3D_{cj}^2\rho_o^3\rho_{cj}\left(\frac{\rho_{cj}}{\rho_o}\right)^{\frac{4}{5}} + 3P_o\rho_o^2\rho_{cj}\left(\frac{\rho_{cj}}{\rho_o}\right)^{\frac{4}{5}} - 4D_{cj}\rho_o^4\left(\frac{\rho_{cj}}{\rho_o}\right)^{\frac{4}{5}}\right)}{9\rho_{cj}^3} \tag{4}$$

This functional form has the thermodynamically correct behavior in the limit of low densities and also agrees with historic data for the CJ detonation speed. It is a 'bad' enough prior so that the Bayesian approach can improve it and it will not be initially stuck in a local minimum.

4.1.2 | Gamma

The Grüneisen gamma was modeled as invariant with density. The prior for the Gamma term was $\Gamma(\rho) = 0.734$, which was obtained as the value of Grüneisen gamma at the CJ state from the thermo-chemical code.

4.2 | Experiments

There were seven different sets of experimental data which were each inverted independently.

4.2.1 | Pemberton 2011

This was a series of six shots performed for standard cylinders of PBX 9501, though only five shots yielded good data [23]. Each shot was instrumented with eight PDV probes. A separate inversion was performed for each

[4] The reciprocal of density.

shot, using the data from all eight probes to inform the inversion. There were five cylinder test shots which were given the designations K12-17229, K12-17230, K12-17231, K12-17232 and K12-17234.

There were two forms of uncertainty in the data. The post processing of the experimental PDV data gave an uncertainty which was reported with the velocity data. This uncertainty was larger in regions with high acceleration. There was also a time-independent uncertainty of 1% of the velocity which was added to account for bias errors between the probes as well as to provide a lower bound on uncertainty in regions where the PDV uncertainty alone gave unreasonably small values.

4.2.2 | Shot 8–1964

This experiment was a standard cylinder test conducted for PBX 9501 and is described in [24]. This experiment was instrumented with eight probes and all eight probes were used in the analysis. This experiment had tighter controls on the geometry of the metal cylinder and is considered to be the best set of cylinder test data for PBX 9501.

4.2.3 | Shot 8–1932

This experiment was a sandwich test conducted for PBX 9501, and is described in [10]. The sandwich test differed from a cylinder test in that the HE charge was rectangular and placed between two thin copper plates. Since the copper was only bent rather than stretched, as in a cylinder test, the material strength and equation of state models of copper had a much smaller effect on the simulations of this experiment. The experimental data were the time history of the velocity of the plates, similar to that of the cylinder test. The experiment was instrumented with four probes. Only a single probe targeted the center-line of the experiment, where the flow was undisturbed by edge effects. This single probe was used for data. The constant uncertainty had to be increased from 1% to 2% in this experiment for the Bayesian calibration process to find a solution.

4.3 | Optimization problem

Each of the seven experiments was its own optimization problem. The objective function was constructed as a Bayesian posterior in the same manner as presented in [10], which used a variational Bayesian procedure [1]. Both the likelihood and prior were modeled as normal distributions, and the response of the simulations to changes to the model degrees of freedom was assumed locally linear. By making these choices and assumptions an efficient posterior maximization procedure was employed which treated the problem as a sequence of quadratic problems which were solved until the change in the log posterior probability was reduced sufficiently between iterations.

$$\log_{10}\left(\mathcal{P}(\theta|\mathcal{Y})\right) = \underbrace{\log_{10}\left(\mathcal{P}(y_{D_{cj}}|\theta)\right) + \sum_{i=1}^{n_{probe}} \log_{10}\left(\mathcal{P}(y_{probe_i}|\theta)\right)}_{\text{likelihood}} + \underbrace{\log_{10}\left(\mathcal{P}(\theta)\right)}_{\text{Prior}} \tag{5}$$

The probability distribution for both the prior and likelihood was chosen to be a multivariate Gaussian, for reasons described in [1].

The resulting optimization problem was given as:

$$\begin{aligned} &\max. : \log_{10}(P(\theta|Y)) \\ &\text{w.r.t. } :\theta \\ &\text{s.t. : } \begin{cases} P(V,\theta) > 0 \forall V \in [0.25\ \text{cm}^3\text{g}^{-1},\ 100.0\ \text{cm}^3\text{g}^{-1}] \\ \frac{\partial P(V,\theta)}{\partial V} < 0 \forall V \in [0.25\ \text{cm}^3\text{g}^{-1},\ 100.0\ \text{cm}^3\text{g}^{-1}] \\ \frac{\partial^2 P(V,\theta)}{\partial V^2} > 0 \forall V \in [0.25\ \text{cm}^3\text{g}^{-1},\ 100.0\ \text{cm}^3\text{g}^{-1}] \end{cases} \end{aligned} \tag{6}$$

The three constrains came from the fact the the pressure on the isentrope must be positive, monotonically decreasing in specific volume, and be convex in specific volume if there is no phase change occurring [22].

Each optimization was run in parallel on 15 High Performance Computing (HPC) nodes each with a dual socket 2.1 GHz 18 core Intel Broadwell processor for up to 12 hours for a total of 5760 processor hours of computing power. For all seven cylinder tests this took 4.6 processor-years.

4.4 | Uncertainty

The degrees of freedom of the isentrope model, θ, were associated with the principal eigen-functions of the prior (see [1, 10] for details on how these eigen-functions were determined). Using the Laplace approximation, a co variance matrix in eigen-function coefficients could be created. This covariance matrix could be projected into a covariance matrix of pressures evaluated on an arbitrary grid of densities using the approach described in Appendix A of this paper. This was done using a regular grid of 100 values of density evenly spaced from 0.01 $\text{g}\,\text{cm}^{-3}$ to 4 $\text{g}\,\text{cm}^{-3}$. The mean, and correlated uncertainty matrix, from the posterior isentrope were used in the subsequent calibration of the Davis Products model.

5 | DAVIS PRODUCTS MODEL CALIBRATION

The inverted isentropes were only one part of the heterogeneous data-set which was used to calibrate the seven free parameters in the Davis Products EOS model, the functional form for this model is given in Appendix B. The hugoniot data from Fritz and Pittman informed the model for pressures above CJ, and the sound speed data from Fritz also helped constrain the off-isentrope behavior. The temperature of HE detonation products is challenging to measure and there were no data which constrained the temperature-related term C_v. The thermo-chemical code was used to generate an isotherm at T_{CJ} to provide data which was sensitive to the temperature model. Similarly, the CJ pressure and temperature, also challenging properties to measure experimentally, were taken from magpie and included in the analysis.

All of these different heterogeneous datasets were combined into a single Bayesian objective function and, again, used multivariate Gaussian distributions for both the prior and likelihood. Additional details of these two probability models are given in Sections 5.1. and 5.2. respectively.

The resulting constrained optimization problem was:

$$\begin{aligned} \text{max.}: \quad & \log_{10}(\mathcal{P}(\Theta|\mathcal{Y})) \\ \text{w.r.t.}: \quad & \theta = \{a,\, k,\, v_c,\, p_c,\, n,\, b,\, C_v\} \\ \text{s.t.}: \quad & k > 1 \\ & n > 1 \\ & a > 0 \\ & b > 0 \\ & v_c > 0 \\ & p_c > 0 \\ & C_v > 0 \end{aligned} \tag{7}$$

This problem was also solved using a variational Bayesian method [1]. It took only two minutes so solve this problem on a single core of a 2.1 GHz Intel Broadwell processor. This six order of magnitude reduction in computational cost allowed much more experimentation in the choice of experiments and the hyper-parameters governing the posterior probability. This was the main motivation for separating the cylinder test inversion and model calibration problems.

5.1 | Likelihood

The set of all data $\mathcal{Y}$ used to compute the posterior probability, (5), consisted of several different kinds of data.

- A CJ isentrope, P(V), resulting from each of the 7 inversion problems from V_{cj} to $10V_o$. The uncertainty was estimated by the UQ process described in Section 4.4.
- The CJ state from magpie consisting of a detonation speed, pressure and temperature. The detonation speed has been adjusted to match the mean of the density adjusted data from [12].
- The pressure along the T_{CJ} isotherm, P(V), obtained from magpie thermo-chemical code from $1.8\,\mathrm{g\,cm^{-3}}$ to $3.25\,\mathrm{g\,cm^{-3}}$.
- The overdriven Hugoniot from [7] for PBX 9501, with experimentally measured uncertainties.
- The Hugoniot from [6] for PBX 9501, with experimentally measured uncertainties.
- The Sound speed data from [6] for PBX 9501, with experimentally measured uncertainties.

The only arbitrary uncertainties assigned to the experimental data were for the isotherm and the CJ state. The uncertainties for the CJ pressure and temperature were $\pm 10\%$, while the uncertainties for the CJ detonation speed was significantly tighter $+/-0.09\%$ or $7.93\,\mathrm{m\,s^{-1}}$. The uncertainty in the isotherm was a constant 5 GPa. Initial tests using just these choices could not identify a model which was a good fit to all the data. Due to biases between the various heterogeneous datasets, there was not a model which was a good fit using the reported uncertainty in the data. Additional hyper-parameters were added to the analysis to scale the magnitude of the uncertainties, these are given in Table 1.

These hyper-parameters for the Bayesian analysis were essentially tuned to produce a reasonable posterior means and covariance. Further justification of these choices will be given in Section 6.3.

5.2 | Prior

The mean of the prior for the Davis Products EOS model was taken from a previous calibration [25], a constant bias of 2% was added to each parameter to prevent the optimization from converging to the local optimum of this existing calibration and to perform a more thorough search of the parameter space. As this calibration had no associated uncertainty, a fractional uncertainty of 53% in each parameter was chosen. This was an additional

hyper-parameter in the Bayesian analysis which was tuned based on the observed variations in the posterior.

6 | RESULTS

The results from the cylinder test inversions are shown in section 6.1. The results from the Bayesian calibration of the model parameters are shown in Section 6.2. The uncertainty quantification study is discussed in Section 6.3.

6.1 | Inversions

Each shot was inverted independently. The data from each shot consisted of one or more time-histories of the wall velocity. The data from each inversion are shown in Figure 1. The models corresponding to the mean of the posterior distribution show excellent agreement with the experimental data in each case.

Further details of the inversion process are given in Table 2 which shows how the CJ state as well as the adiabatic and Grüneisen gamma differed for each shot. For each inversion the CJ detonation speed of the optimal isentrope agreed closely with the target historical value $8.810\,\mathrm{km\,s^{-1}}$. Additionally, the adiabatic gamma for each shot was close to the theoretical value of $\frac{6}{5}$. This is important as the cylinder test does not extend down to very low pressures and this exponent ensures the isentropes can extrapolate outside the regime of the B-splines in a physically meaningful way. The greatest shot-to-shot difference was the optimal value of the Grüneisen gamma. The fact that the Grüneisen gamma varied so significantly shot-to-shot showed the importance of including this variable in the analysis as it allowed the flexibility for the isentrope to truly model the isentropic expansion of the gases rather than also attempt to fit any non-ideal behavior.

TABLE 2 Comparison of the CJ state of the model corresponding to the mean of the posterior as well as the adiabatic gamma (γ) and Grüneisen gamma (Γ).

Shot	P_{cj} GPa	D_{cj} km s^{-1}	e_{det} kJ g^{-1}	γ –	Γ –
Prior	**35.7869**	**8.8100**	**5.4989**	**1.209**	**0.720**
K12-17229	34.0757	8.8095	5.3406	1.209	2.380 ± 0.051
K12-17230	34.5208	8.8086	5.3202	1.209	3.215 ± 0.072
K12-17231	36.5087	8.8034	5.3189	1.209	3.324 ± 0.070
K12-17232	34.6696	8.8079	5.3156	1.209	0.605 ± 0.071
K12-17234	34.3100	8.8054	5.4299	1.209	0.275 ± 0.060
8-1932	35.9102	8.8107	5.2400	1.209	1.571 ± 0.063
8-1964	36.3470	8.8081	5.3605	1.203	0.000 ± 0.072

6.2 | Parametric model calibration

The result of the Bayesian analysis of the Davis Products model parameters was a mean and covariance matrix for a multivariate normal posterior distribution. Properties of the CJ state from the Davis model with parameters taken from the mean of the posterior distribution are shown in Table 3, and simulations using this Davis model are compared to the various experimental datasets are shown in Figures 2 and 3.

The CJ state shows good agreement with the magpie results and historical data. The detonation speed agreed most closely, as it was the most constrained property (see Section 5.1.), while the pressure and temperature agree within 10%.

Simulations of the experiments used to constrain the Davis products EOS parameters are shown in Figures 2 and 3. Overall, all four types of experiments show very close agreement with the experimental data. In both the hugoniot and isentrope data, the thermodynamic locus predicted by magpie is also shown. This data was not used in the optimization but is provided for reference. In Figure 2 it is important to note that the prior coefficients were perturbed from the previous PBX 9501 calibration [25] and the poor agreement of the prior with the experiments is not reflective of this calibration.

At low pressures, the single sandwich test experiment, shot 8–1932, shown in Figure 3, was a notable outlier from the other isentropes. The sandwich experiment did not examine densities as low as the cylinder tests. Figure 1f shows that the time history was much shorter than for cylinder tests and, additionally, the density decreased linearly with wall displacement for a sandwich test rather than with the square of the displacement for in the axi-symmetric cylinder tests. For these reasons, the isentrope for shot 8–1932 is poorly constrained at large range of volumes examined in Figure 3. However,

TABLE 3 Comparison of the mean of the posterior from the Davis Products EOS calibration to the Magpie predictions.

Value	Posterior	magpie	
Pressure	35.97666	33.7656	GPa
Density	2.45493	2.40612	g cm^{-3}
Temperature	3221.62	3247.51	K
Shock speed	8.81604	8.81000	km s^{-1}
Particle speed	2.22267	2.08749	km s^{-1}

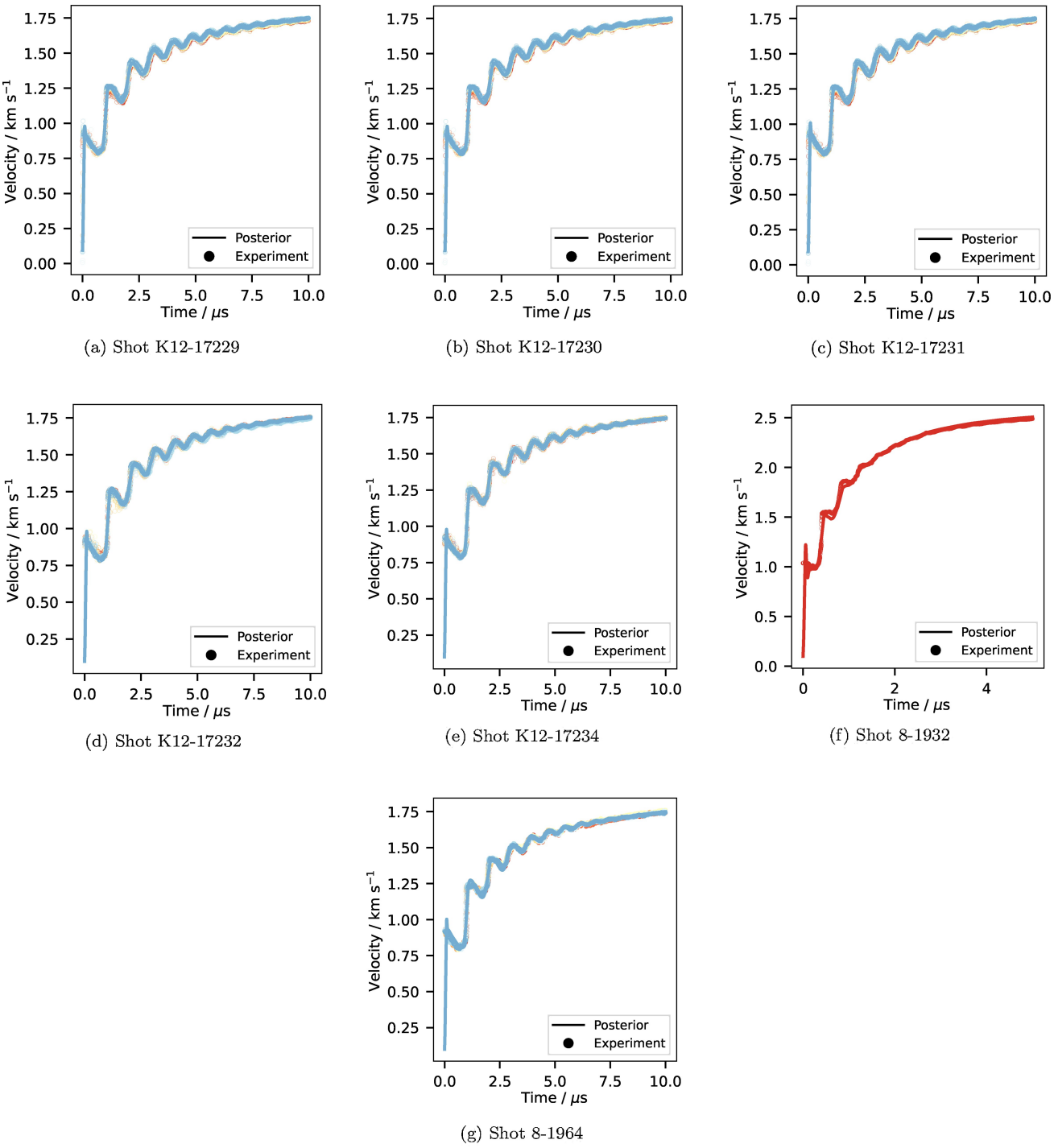

FIGURE 1 The wall velocity as a function of time is shown for all experimental probes and is compared to the corresponding simulation output. Each shot was measured by eight probes (except shot 8–1932) and the simulations and experimental data from each probe share the same color. The simulation used the model corresponding to the mean of the posterior.

it is important to note that over the specific volume range where both cylinder- and sandwich- test experiments provided data, the results from all six isentropes are in close agreement. The behavior of the cylinder test was much more dependent than the sandwich test on the EOS and strength models used for the confining material. The fact that these isentropes are in such close agreement indicates that the choices made in modeling the copper were sound and did not significantly influence the results.

One major assumption in using the inverted isentropes as a surrogate for cylinder tests was that the

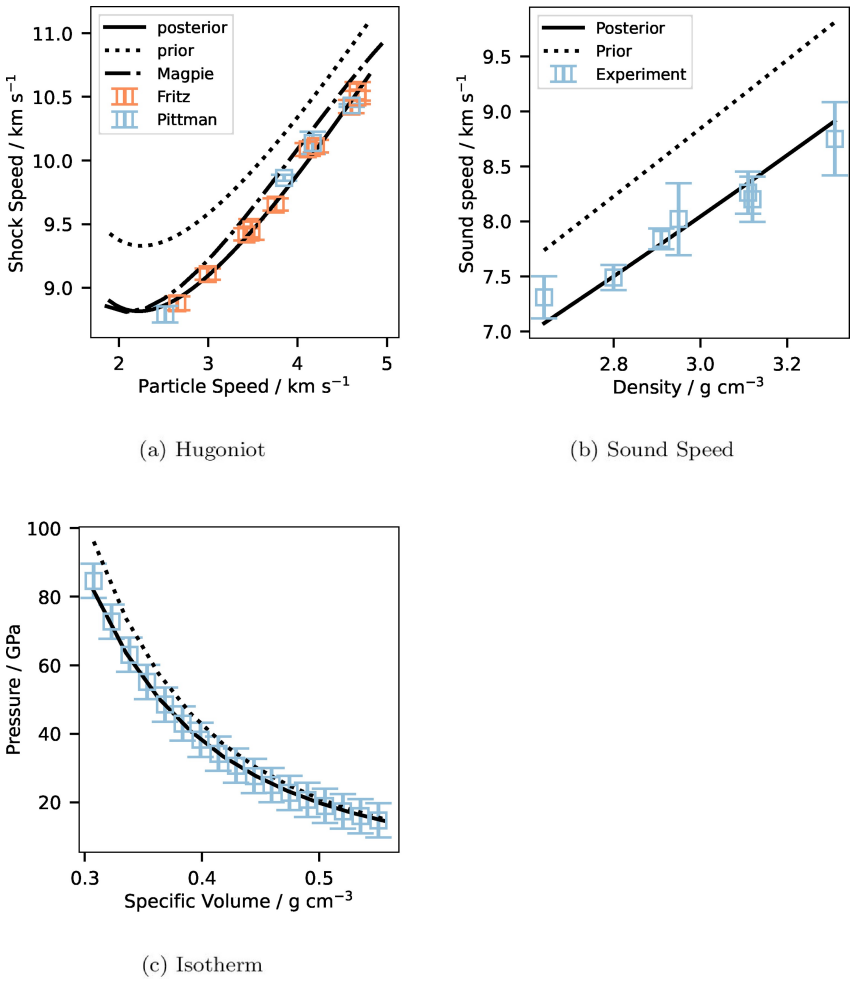

(a) Hugoniot

(b) Sound Speed

(c) Isotherm

FIGURE 2 Comparison of the calibration data to simulations using the Davis products model with coefficients taken from the mean of the posterior distribution. (a) experimental overdriven Hugoniot measurements in $U_s - u_p$ form [6, 7]. Note, the magpie Hugoniot is shown on this figure for reference but was not used in the calibration. (b) experimental sound speed as function of density [6] (c) temperature along the isotherm from Magpie in P(V) form.

posterior model would be able to make good predictions of cylinder test experiments. To test this assumption, shot K12-17234 was run again using a Davis products EOS with parameters from the mean of the posterior distribution. These results are shown in Figure 4 along with a simulation of the same experiment using an EOS defined by a SESAME [18] table generated by magpie. The simulation using the calibration from the mean of the posterior showed excellent agreement with experiments, validating the posterior model and demonstrating the utility of using inverted isentropes as a surrogate for hard-to-simulate dynamic experiments.

Re-examining the magpie results shown in Figures 2a, 3 and 4, the thermo-chemical code does not do as good a job matching experimental data as the calibration. It is important to note the *only* input to magpie is the chemical composition of the HE and binder, and from this it can make predictions which are remarkably close to experiments. The current approach shows how these results can be augmented to make better predictions of experiments. The thermo-chemical code is still critical in providing data that is not accessible experimentally, such as the isotherm, as well as in cases where there are fewer experimental data available.

6.3 | Uncertainty Quantification

By structuring the problem in a Bayesian manner, information about both the mean and covariance of the posterior distribution can be obtained from the experimental data. The Laplace approximation was used to calculate the posterior covariance for the Davis EOS parameters.

The first way this covariance matrix was examined was to decompose the matrix into a diagonal matrix of

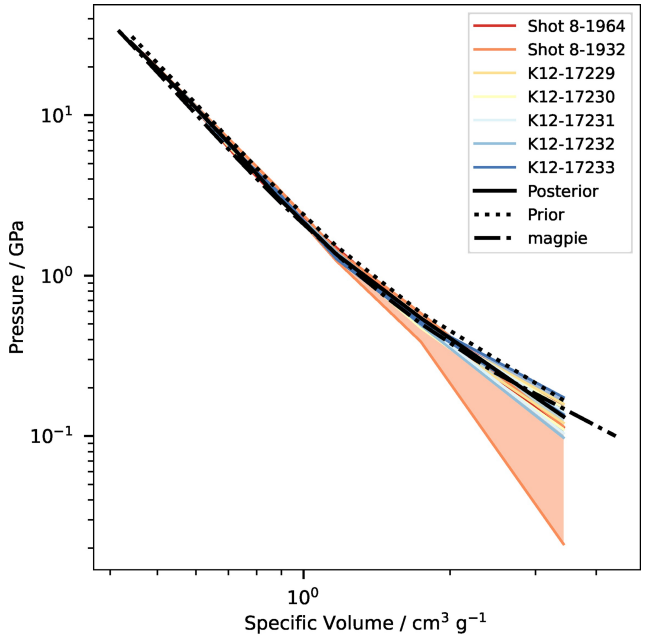

(a) Full domain

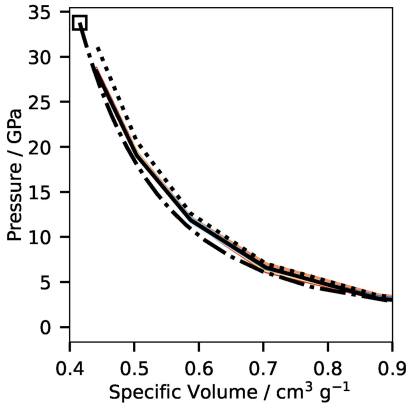

(b) Near CJ state

FIGURE 3 Comparison of the calibration data to simulations of the inverted isentrope using the Davis products model with coefficients taken from the mean of the posterior distribution. Though it was not used in the calibration, the magpie isentrope is also shown on this figure for reference.

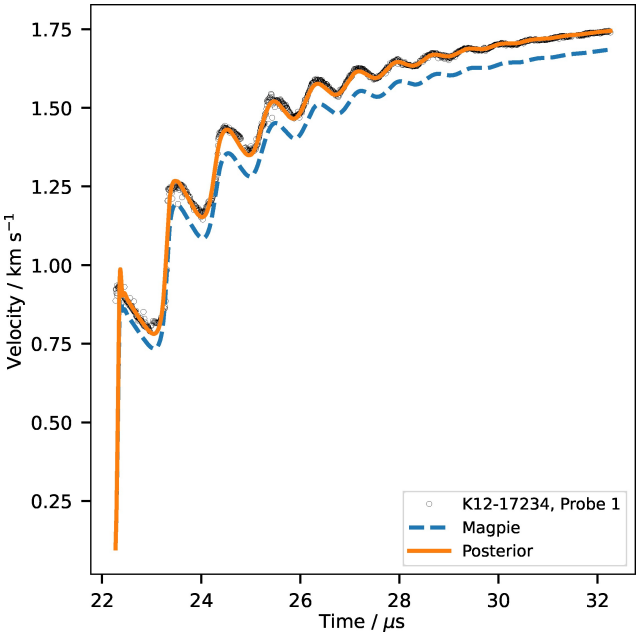

FIGURE 4 Shot K12-17234 simulated using the initial magpie model as well as the mean of the posterior for the Davis Products EOS model parameters.

marginal uncertainties and a correlation matrix. This correlation matrix is shown in Figure 5, the horizontal and vertical axes are labeled by model parameters, whose relationship to the overall EOS model is described in Appendix B. The correlation plot has a diagonal of one and the correlation between the model parameters is shown as a dimensionless value between a full positive correlation of 1 and full negative correlation of −1.

The correlations shown in this Figure highlight the behavior of the model. The parameters a, k, v_c, p_c and n all control the shape of the isentrope, therefore it is unsurprising that they are all strongly correlated. The parameter b controls the off-isentrope behavior, and was strongly correlated with the isentrope parameters. The final term C_v was weakly correlated with all the other parameters, it controls the temperature relationship in the EOS. The weak correlation with the other parameters shows why it was critical to include the isotherm data from the thermo-chemical code in the analysis. Otherwise this term would have been very weakly constrained by the experimental data.

Another way to examine the posterior distribution is to draw samples from the distribution and characterize their behavior. Davis products EOS parameter sets were drawn from the posterior using standard methods for sampling from a normal distribution. For each of these samples the value of D_{cj} was computed and corrected to a one-inch diameter and then a Cumulative Density Function (CDF) for this Quantity of Interest (QOI) was constructed and is shown in Figure 6. In addition to the CDF of the posterior, the CDF of the experimentally observed detonation speeds was also computed and shown in Figure 6. The two CDFs are qualitatively very similar. Quantitatively, the integral of the area between the two (computed using the area metric of [26]) is 0.6214 standard deviations giving further evidence of the close agreement between the CDFs.

The agreement between the two CDFs was the metric by which the hyper-parameters of the analysis were

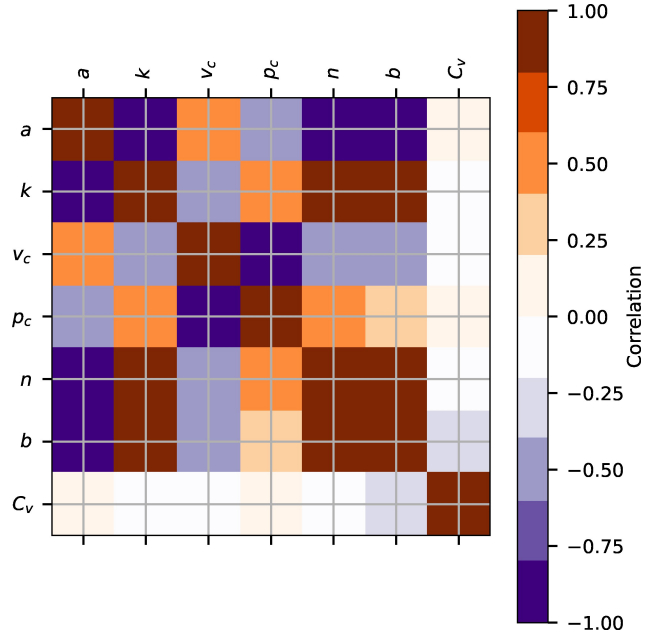

FIGURE 5 Correlation between the model degrees of freedom for the Davis product EOS model. This figure shows the strong correlation of all the parameters controlling the shape of the reference curve.

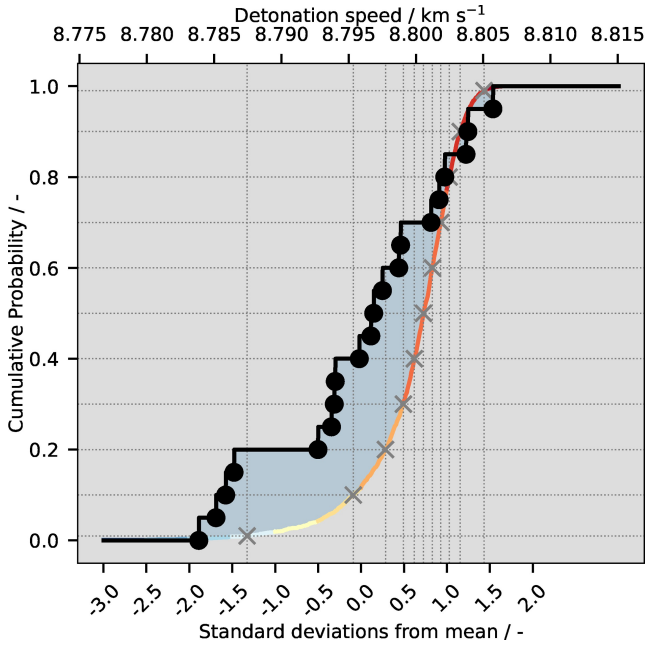

FIGURE 6 Posterior samples, sorted by D_1, the eleven percentile points are shown in the plot. The black dots are the cumulative probability distribution of experimentally observed detonation speeds, corrected to 1.836 g cm^{-3} for charges with a diameter of one inch or greater. The D_1 is scaled by $\mu = 8.7959$ km s^{-1} and $\sigma = 0.0064$ km s^{-1}.

adjusted. Though there are other methods to select these hyper-parameters, tuning the hyper-parameters yielded a

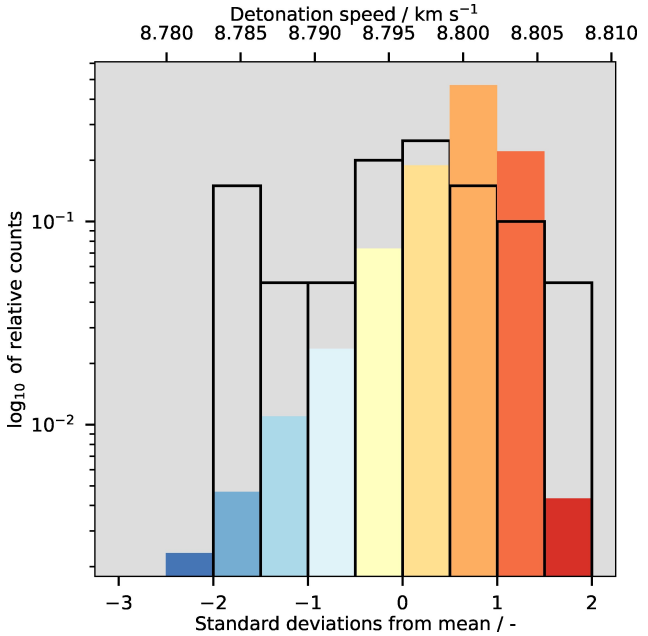

FIGURE 7 The resulting histogram of D_1 found from sampling the posterior. The hollow bars are the experimental data and the filled bars are the sampled results. On the lower axis D_1 is scaled by $\mu = 8.7959$ km s^{-1} and $\sigma = 0.0064$ km s^{-1} and on the top axis D_1 is shown in km s^{-1}.

distribution which shows the same degree of variation as the experimental observations. Additionally, each sample in the posterior CDF was a point which was plausible given all the experimental data. This final point is critical as Figure 5 shows, all the parameters are highly correlated, where some correlations are positive and some negative. A simple scaling of the Davis parameters to vary the detonation speed would not give plausible models with respect to all the other data which are affected by the calibration. A sampling method is the only way to discover plausible models with the expected variation in detonation speed.

The posterior and experimental distributions of D_1 are again compared in Figure 7, where a histogram of the posterior samples and experimental data are shown. There are a small number of samples which yield a detonation speed slower than any experimental observations, but overall, there are posterior samples for the full range of detonation speeds observed experimentally. The relationship between the detonation speed and the shape of the isentrope is shown in Figure 8. Here the CJ isentrope for the parameter sets corresponding to 1000 posterior samples are shown and the isentropes are colored according to their detonation speed. The first thing to note is that the isentropes are all extremely similar for specific volumes less than 2×10^{-3} m^3 kg^{-1} (density greater than 0.5 g cm^{-3}). The spread in the isentropes at large specific volumes was noticeable, the isentropes corresponding to

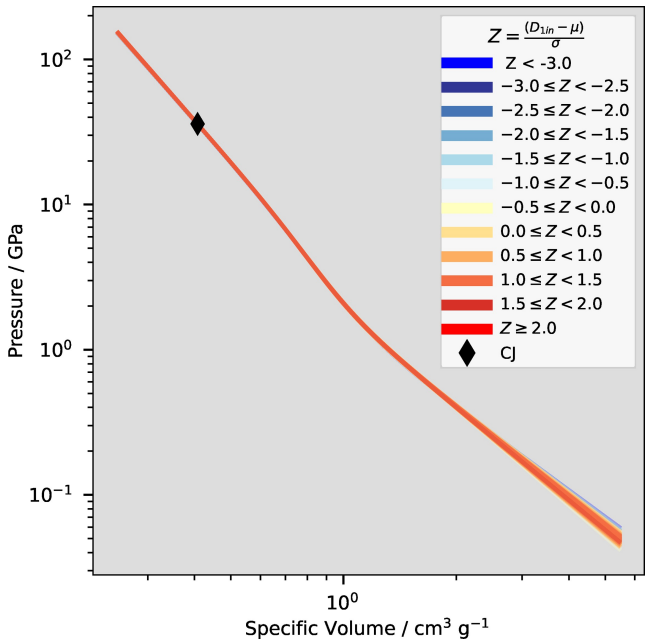

FIGURE 8 CJ isentropes of the models corresponding to the posterior samples. The isentropes are colored by the bins from the histogram in Figure 7. The D_1 is scaled by $\mu = 8.7959\ \mathrm{km\,s^{-1}}$ and $\sigma = 0.0064\ \mathrm{km\,s^{-1}}$.

the highest detonation speeds were clustered together while those corresponding to the lower detonation speeds occurred both above and below this trend. It is important to note that the trend of detonation speed was not monotonic with respect to the isentropes, again showing why a sampling method was required to obtain a distribution in detonation speeds, rather than simply scaling a baseline isentrope shape.

Using the CDF, parameter sets representing the 1^{st}, 10^{th}, 20^{th}, 30^{th}, 40^{th}, 50^{th}, 60^{th}, 70^{th}, 80^{th}, 90^{th} and 99^{th} percentiles of the detonation speed were reported in Table 4. These parameter sets can be used in conjunction with a hydrodynamic simulation code to explore the effects of the inherent variability in the properties of an explosive on some quantity of interest in the simulation. The relative difference in these simulations was small so any QOI which is not extremely sensitive to detonation speed may not show a significant difference. However, these calibrations are valuable in that they can be used to show that the inherent variation observed in real HE does not affect a result.

In Section 4.1. it was noted that the expected asymptotic behavior of the isentrope at large volumes was a power law with a slope of $\frac{6}{5}$. In the Davis products EOS model, the asymptotic behavior is governed by the term k and in Table 4 the value of k is consistently larger than this value. It was not possible to identify a model which had the desired asymptotic behavior while fitting all the

TABLE 4 Davis Products EOS calibrations for various percentiles in D_{cj}. Previous calibrations are also shown for reference.

%	D_{cj} km s^{-1}	a –	b –	C_v km^2 s^{-2} K^{-1}	e_{det} km^2 s^{-2}	k –	n –	p_c GPa	v_c cm^3 g^{-1}
Aslam [25]	8.8110	6.843 11×10^{-1}	1.250	7.30×10^{-4}	5.60208	1.621	1.589	5.388 97	7.458 29×10^{-1}
0.01	8.787	4.883×10^{-1}	1.415	9.803×10^{-4}	5.231	1.944	2.682	3.956	8.203×10^{-1}
0.10	8.795	4.724×10^{-1}	1.474	9.078×10^{-4}	5.222	1.978	2.775	4.022	8.165×10^{-1}
0.20	8.798	3.941×10^{-1}	1.848	8.134×10^{-4}	5.075	2.162	3.263	4.142	8.084×10^{-1}
0.30	8.799	4.096×10^{-1}	1.802	8.575×10^{-4}	5.090	2.128	3.190	3.951	8.207×10^{-1}
0.40	8.800	4.526×10^{-1}	1.573	9.043×10^{-4}	5.168	2.029	2.852	3.981	8.191×10^{-1}
0.50	8.801	4.470×10^{-1}	1.582	1.013×10^{-3}	5.176	2.038	2.893	4.018	8.172×10^{-1}
0.60	8.801	4.267×10^{-1}	1.592	9.140×10^{-4}	5.104	2.093	3.025	3.926	8.222×10^{-1}
0.70	8.802	4.436×10^{-1}	1.701	9.788×10^{-4}	5.136	2.055	2.893	3.974	8.191×10^{-1}
0.80	8.802	4.385×10^{-1}	1.594	9.934×10^{-4}	5.162	2.058	2.958	4.097	8.117×10^{-1}
0.90	8.803	4.191×10^{-1}	1.723	9.649×10^{-4}	5.102	2.108	3.105	3.974	8191×10^{-1}
0.99	8.805	4.274×10^{-1}	1.616	8.811×10^{-4}	5.123	2.088	3.081	4.030	8.152×10^{-1}

available experimental data. As can be seen in Figure 5, the parameter k is highly correlated with all other model parameters and cannot be adjusted independently. k is the polytropic gas coefficient for large expansions on the CJ isentrope, but the experimental data appears not to contain the large-expansion regime where the EOS exhibits polytropic gas behavior. This reduces k to a fitting parameter, where it has lost its original physical meaning. This demonstrates the challenge of using a mathematical function with finite degrees of freedom to represent a real physical process where sufficient experimental data to constrain the model may not be available. Additionally, though the value of k is higher than physically expected, it is part of a pysically meaningful calibration within the range of available experimental expansion data, and the isentropes remain integrable functions as $V \to \infty$.

7 | CONCLUSIONS AND FUTURE WORK

This paper sought to quantify the uncertainty in the parameters of the Davis Products EOS model for the HE PBX 9501. A four step approach was used. First, historical data was used to identify the best value for the detonation speed D_{cj}, which was used to anchor the subsequent steps. Second, a thermo-chemical code magpie was used to identify hard to measure properties of the CJ state. Third, a Bayesian inverse problem was used to find a function $P(\rho)$ from experimental observations of the wall velocity of seven different dynamic experiments. Finally, the data from the thermo-chemical code, the $P(\rho)$ functions and all other available historical data were combined into a Bayesian calibration problem where the optimal set of Davis Products EOS parameters was identified. In addition to this mean value, a covariance matrix in Davis Products EOS parameters was found and was used to examine the expected variation of the property D_1 given the available data. The variation in the model parameters led do a variation in D_1 which was similar to the variations observed in historical experimental measurements of this quantity. Eleven set of Davis Products EOS parameters were taken from the posterior distribution representing different percentile levels of D_1. These parameter sets can be used in future uncertainty quantification assessments to show the effect of uncertainty in the true detonation speed of the material.

This study was confined to examining the material PBX 9501. This is one of the most studied precision HE materials in existence. Other HE materials have much less data, especially rate stick data which was used to asses if the variation of D_1 in the posterior was in agreement with experiment. This study had a range of adjustable hyper-parameters which were tuned to bring the posterior distribution of D_1 into agreement with experiments. The choices of these hyper-parameters could be used to inform a similar study of a different HE for which fewer data are available.

The fact that the hyper-parameters in the analysis were tuned to the data is a weakness in the analysis methodology. A hierarchical Bayesian method could infer the optimal values of the hyper parameters alongside the model parameters. Additionally, while the variational Bayesian method was required for the computationally expensive inverse problem of cylinder tests, the Davis products EOS calibration was constitutionally simple enough that it could be solved using a sampling based technique such as Markov-Chain Monte-Carlo. Both these approaches would be excellent avenues for future work.

This work converted all the experimental and theoretical data available about the HE PBX 9501 into both a single *best* calibration of the Davis Products EOS model as well as an ensemble of calibrations which span the expected variation in the important performance metric, the CJ Detonation Velocity.

Nomenclature

Symbols

γ Adiabatic gamma [−]
p Density [$\mathrm{kg\,m^{-3}}$]
θ Vector of model parameters [−]

Variables

A Prior fitting coeflicient [−]
a Davis products isentrope parameter [−]
n Davis products isentrope parameter [−]
B Prior fitting coeflicient [−]
b Davis products Grüneisen parameter [−]
C_v Specific heat capacity at constant volume [$\mathrm{J\,kg^{-1}\,K^{-1}}$]
D_1 Detonation speed for a one-inch (25.4 mm) diameter charge [$\mathrm{m\,s^{-1}}$]
D_{cj} Thermodynamic detonation speed for a charge of infinite diameter [$\mathrm{m\,s^{-1}}$]
e_{det} Energy released by detonation [$\mathrm{J\,kg^{-1}}$]
k Davis products isentrope parameter [−]
$\mathcal{P}$ Probability [−]
P Pressure [Pa]
Pc Davis products critical pressure [Pa]
R Rayleigh Line [−]

u_p Particle speed [m s^{-1}]
U_s Shock speed [m s^{-}]
V_c Davis products critical volume [m^3 kg^{-1}]
V Specific volume [m^3 kg^{-1}]
$\mathcal{Y}$ Vector of experimental data [−]

Modifiers

$_{cj}$ Property of the CJ state [−]
$_0$ Property of the reactants state [−]

Appendix A: Uncertainty in isentrope functions

The isentrope used in the cylinder test inversion was represented as a B-spline.

The inverse problem operated in a space θ where $\theta = cT$, where T was a transformation matrix obtained using methods computed in Appendix B of and c are the coefficients for the B-spline basis functions.

The basis functions of the B-splines could be evaluated on arbitrary grids of density and combined into a basis matrix

$$\mathbf{B}(\rho) = [\, b_1(\rho) \quad b_2(\rho) \quad \ldots b_n(\rho)\,] \tag{8}$$

Applying the Laplace approximation to the posterior of the inverse problem yields a covariance matrix in the degrees of freedom θ. This can be transformed into a covariance matrix in pressure-density space by,

$$\Sigma_P(\rho) = B(\rho)T\Sigma_\theta T^T B(\rho)^T. \tag{9}$$

Appendix B: Davis Products equation of state model

The Davis Products equation of state is a Mie-Grüneisen EOS model with equations for both temperature and pressure as a function of the thermodynamic quantities of density and mass-specific internal energy.

$$P(\rho, e) = P_s(\rho) + \rho\Gamma(\rho)(e - e_s(\rho)) \tag{10}$$

$$T(\rho, e) = T_s(\rho) + \frac{1}{C_v}(e - e_s(\rho)) \tag{11}$$

The functional form of the reference curve is:

$$P_s(\rho) = P_c \frac{\left(\frac{(\rho v_c)^{-n}}{2} + \frac{(\rho v_c)^n}{2}\right)^{\frac{a}{n}}}{(\rho v_c)^{-(k+a)}} \frac{k - 1 + F(\rho)}{k - 1 + a}, \tag{12}$$

where,

$$F(\rho) = \frac{2a(\rho v_c)^n}{(\rho v_c)^{-n} + (\rho v_c)^n}. \tag{13}$$

The energy on the reference curve can be obtained by integrating (12) to obtain:

$$e_s(\rho) = \frac{P_c v_c}{k - 1 + a} \frac{\left(\frac{(\rho v_c)^{-n}}{2} + \frac{(\rho v_c)^n}{2}\right)^{\frac{a}{n}}}{(\rho v_c)^{-(k-1+a)}}. \tag{14}$$

The Gr“uneisen gamma from (10) is modeled as being a function of density only

$$\Gamma(\rho) = k - 1 + (1 - b)F(\rho) \tag{15}$$

The temperature on the reference curve is given as:

$$T_s(\rho) = \frac{2^{\frac{-ab}{n}}}{k - 1 + a} \frac{P_c v_c}{C_v} \frac{\left(\frac{(\rho v_c)^{-n}}{2} + \frac{(\rho v_c)^n}{2}\right)^{\left(\frac{a}{n}(1-b)\right)}}{(\rho v_c)^{-(k-1+a(1-b))}}, \tag{16}$$

ACKNOWLEDGMENTS

The authors would like to thank the developers of the following open source software packages which were used in the preparation of this manuscript: matplotlib [27], numpy [28], and scipy [29]. This work was supported by the U.S. Department of Energy through the Los Alamos National Laboratory. Los Alamos National Laboratory is operated by Triad National Security, LLC, for the National Nuclear Security Administration of U.S. Department of Energy (Contract No. 89233218CNA000001). Approved for public release LA-UR-23-24589 and DOPSIR 23-S-1920.

DATA AVAILABILITY STATEMENT

Research data are not shared.

ORCID

Stephen A. Andrews http://orcid.org/0000-0003-4997-3906
Jeffery A. Leiding http://orcid.org/0000-0003-2512-5291
Jasper Thrussell http://orcid.org/0009-0009-8378-6419
Christopher Ticknor http://orcid.org/0000-0001-9972-4524

REFERENCES

1. S. A. Andrews, A. M. Fraser, *ASME J. Verif. Validation Uncertainty Quantif.* **2019**, *4*, 011002-1–01102-15.
2. W. C. Davis, *11th International Detonation Symposium*, Snowmass, CO, **1998**, 1–7.

3. W. C. Davis, *10th Detonation Symposium*, Boston, MA, **1993**, 1–19.
4. W. C. Davis, *8th Symposium on Detonation*, Albuquerque, NM, **1985**, 1–12.
5. T. D. Aslam, *J. Appl. Phys.* **2018**, *123*, 145901.
6. J. N. Fritz, R. S. Hixson, M. S. Shaw, C. E. Morris, R. G. McQueen, *J. Appl. Phys.* **1996**, *80*, 6129–6141.
7. E. R. Pittman, C. R. Hagelberg, R. L. Gustavsen, T. D. Aslam, *AIP Conf. Proc.* **2018**, *1979*, 150032.
8. R. Catanach, L. Hill, H. Harry, E. Aragon, D. Murk, *Los Alamos National Laboratory*, Los Alamos, NM, **1999**, LA 13643-MS.
9. G. I. Taylor, *Civil Defence Research Committtee, Ministry of Horne Security* **1941**.
10. S. A. Andrews, A. M. Fraser, S. I. Jackson, E. K. Anderson, *ASME Verification and Validation Symposium*, Las Vegas, NV, **2019**,1–13.
11. C. Ticknor, S. A. Andrews, J. A. Leiding, *AIP Conf. Proc.* **2020**, *2272*, 030033.
12. T. D. Aslam, M. Short, *Los Alamos National Laboratory*, Los Alamos, NM, **2013**, LA-UR-1326358.
13. L. Hill, *Los Alamos National Laboratory*, Los Alamos, NM, **2012**, memorandum.
14. A. W. Campbell, R. Engelke, *6th symposium (international) on Detonation*, Coronado CA, **1976**, 642–652.
15. L. Fried, P. Souers, *Lawrence Livermore National Laboratory*, Livermore, CA, **1994**, UCRL-ID-117240.
16. M. Ross, *J. Chem. Phys.* **1979**, *71*, 1567–1571.
17. J. D. Coe, J. T. Gammel, *Los Alamos National Laboratory*, Los Alamos, NM, **2016**, LA-UR-16-26877.
18. S. P. Lyon, J. D. Johnson, *Los Alamos National Laboratory*, Los Alamos, NM, **1992**, LA-UR-92-3407..
19. D. E. Burton, *SAMGOP-94 2nd International Workshop on Analytical Methods and Process Optimization in Fluid and Gas Mechanics*, Holiday Base, Arzamas-16, Russia, **1994**.
20. P. A. Rigg, M. D. Knudson, R. J. Scharff, R. S. Hixson, *J. Appl. Phys.* **2014**, *116*, 033515.
21. D. L. Preston, D. L. Tonks, D. C. Wallace, *J. Appl. Phys.* **2003**, *93*, 211–220.
22. R. Menikoff in: *Shock Wave Science and Technology Reference Library, Vol. 2* (Ed.: Y. Horie), Springer, **2007**, 157–188.
23. S. J. Pemberton, T. D. Sandoval, T. J. Herrera, J. A. Echave, G. Maskaly, *Los Alamos National Laboratory*, Los Alamos, NM, **2011**, LA-UR 11–04999.
24. M. A. Zocher, T. D. Aslam, S. I. Jackson, E. K. Anderson, *Proceedings of the 16th international detonation symposium*, Cambridge MD, **2018**, 1–11.
25. T. D. Aslam, M. A. Price, C. Ticknor, J. D. Coe, J. A. Leiding, M. A. Zocher, *AIP Conf. Proc.* **2020**, *2272*, 030001.
26. W. L. Oberkampf, C. J. Roy, *Verification and Validation in Scientific Computing*, Cambridge University Press, Cambridge, UK, **2012**.
27. J. D. Hunter, *Comput. Sci. Eng.* **2007**, *9*, 21–29.
28. C. R. Harris, K. J. Millman, S. J. van der Walt, R. Gommers, P. Virtanen, D. Cournapeau, E. Wieser, J. Taylor, S. Berg, N. J. Smith, R. Kern, M. Picus, S. Hoyer, M. H. van Kerkwijk, M. Brett, A. Haldane, J. Fernandez del Rio, M. Wiebe, P. Peterson, P. Gerard-Marchant, K. Sheppard, T. Reddy, W. Weckesser, H. Abbasi, C. Gohlke, T. E. Oliphant, *Nature* **2020**, *585*, 357–362.
29. P. Virtanen, R. Gommern, T. E. Oliphant, M. Haberland, T. Reddy, D. Cournapeau, E. Burovski, P. Peterson, W. Weckesser, J. Bright, S. J. van der Walt, M. Brett, J. Wilson, K. J. Millman, N. Mayorov, A. R. J. Nelson, E. Jones, R. Kern, E. Larson, C. J. Carey, i. Polat, Y. Feng, E. W Moore, J. VanderPlas, D. Laxalde, J. Perktold, R. Cimrman, I. Henriksen, E. A. Quintero, C. R. Harris, A. M. Archibald, A. H. Ribeiro, F. Pedregosa, P. van Mulbregt, *Nature Methods* **2020**, 261–272.

How to cite this article: S. A. Andrews, J. A. Leiding, J. Thrussell, C. Ticknor, *Propellants, Explos., Pyrotech.* **2024**, *49*, e202300110. https://doi.org/10.1002/prep.202300110

Graphical Abstract

The contents of this page will be used as part of the graphical abstract of html only.
It will not be published as part of main.